

Article

# Effect of NS-DBD Actuator Parameters on the Aerodynamic Performance of a Flap Lifting Device

Kun Chen <sup>1,\*</sup>, Chen-Yao Wei <sup>2</sup> and Zhi-Wei Shi <sup>3</sup>

<sup>1</sup> National Key Laboratory of Transient Physics, NJUST, Nanjing 210094, China

<sup>2</sup> China Academy of Aerospace Aerodynamics, Beijing 100074, China; wchenyao@hotmail.com

<sup>3</sup> Key Laboratory of Unsteady Aerodynamics and Flow Control, NUAU, Nanjing 210016, China; szwam@nuaa.edu.cn

\* Correspondence: 12016120@njjust.edu.cn; Tel.: +86-1519-588-7135

Received: 16 October 2019; Accepted: 28 November 2019; Published: 30 November 2019



**Abstract:** The flap lift device is an important part of the conventional configuration of aircrafts and has an important impact on the aerodynamic performance. In this paper, a high-efficiency, simple, and energy-saving nanosecond dielectric barrier discharge (DBD) plasma actuator is placed in the vicinity of the flap lift device to improve the aerodynamic performance of the flap by controlling the flow field. The two-dimensional airfoil GAW-1 and its 29% flap were selected as the research objects, and the nanosecond (NS) DBD actuators were fixed at different locations near the deflection angle of the 10° flap. The excitation frequency, pulse width, and energy density parameters of the pulse discharge were adjusted, and then, the effects of parameter changes on aerodynamic characteristics of the airfoil were studied by numerical simulation. The simulation results show that adjusting the excitation frequency on the aerodynamic drag is weak and that the effect on the aerodynamic lift is obvious. The increase of the discharge pulse width will have a more significant effect on the flow field, i.e., a proper increase of the discharge pulse width can achieve better drag reduction, and increase lift after a stall at a high angle of attack. Although the increase of discharge energy density can strengthen the pulse perturbation effect on the flow field, it also contributes to some adverse effects and has no obvious optimization effect on the control efficiency of lift increase and drag reduction.

**Keywords:** high lift system; dielectric barrier discharge; plasma; nanosecond pulse; aerodynamic performance

## 1. Introduction

As an important part of aircraft aerodynamic design, the flap lift device affects the take-off and landing performance of the aircraft and is closely related to flight safety, environmental protection, and economy. A mechanical flap lift device usually consists of multi-element airfoils arranged along the chordwise direction, including leading edge slats, leading edge flaps, and trailing edge flaps, etc. To meet the lift requirements for take-off and landing for large aircraft, the flap lift device even has as many as five sections, which makes the control mechanism overly complicated and increases the empty weight. Improving the lift efficiency of the flaps can reduce the number of flap sections and the additional mass.

The dielectric barrier discharge (DBD) plasma actuator, which has received extensive attention in recent years, is able to control the local or global flow field efficiently by using slight and local disturbances [1–3]. Current research on DBD plasma actuators includes active control of separation flow [4], boundary layer transition control [5], pneumatic noise control [6], side force control for the revolution body [7], flight control [8], plasma propulsion [9], flow control in the engine [10], plasma sensors [11], etc.

Compared with the AC-DBD (alternating-current dielectric barrier discharge) actuator, the NS-DBD (nanosecond dielectric barrier discharge) actuator has the advantages of small size, high discharge frequency and high controllable inlet velocity. Many scholars have also carried out research on the control of separation flow by using NS-DBD [12–15]. Rethmel et al. [16] used an NS-DBD actuator to increase the stall angle of attack of the aircraft during the wind tunnel test. From their viewpoint, at a large angle of attack, the actuator will generate a spanwise vortex, thus promoting the mixing of the flow and realizing control of the separation flow. Roupasov et al. [17] carried out research to control the separation flow with a Mach number of incoming flow within the range of 0.05–0.85. The NS-DBD actuator can effectively realize the control of separation flow, lift increase, and drag reduction, as well as noise control at high Mach number. Popov [18] reported the disturbance phenomenon of NS-DBD on the laminar boundary layer by numerical simulation. They believe that the main NS-DBD mechanism is the generation of a T-S disturbance wave, and thus the flow control mechanism of the NS-DBD may include a large-scale vortex, flow transitions, or other factors. Little et al. [19–21], from Ohio State University, used a plasma aerodynamic actuator to conduct a study on simplified flow control of the high lift device. The results show that the plasma actuator with millisecond pulses can effectively control the separation of the boundary layer of the trailing edge flap at a Reynolds number of  $2.4 \times 10^5$ – $7.5 \times 10^5$ . The plasma actuator with nanosecond pulses can only control the separation of the leading edge at a Reynolds number of  $7.5 \times 10^5$ – $1.00 \times 10^6$ , and it is difficult to control the separation of the trailing edge flap. Wang et al. [22] studied the control ability of airfoil flow separation by a millisecond pulse plasma actuator. The results show that the plasma actuator can effectively restrain the flow separation at the leading edge of the airfoil and significantly improve the maximum lift coefficient of the airfoil. The effect is optimal when the flow control is applied simultaneously at the flap and the rear section of the main wing. In this condition, the maximum lift coefficient can be increased by approximately 30%.

Two disturbances generated by NS-DBD are considered as potential mechanisms of flow control, the first is compression wave, the second is vortex structure [23–25]. Leonov et al. [26] believe that NS-DBD will generate random local thermal disturbance near the wall in a relatively long-time scale ( $> 100$  us) after discharge, and will form compression wave in a very short time (1–10 us). Sergey, Unfer, Roupasov, Correale, Little, Adamovich et al. [14,19,20,27,28] suggest that shock wave, which is the dominant factor of flow control, is generated after NS-DBD discharge due to thermal effect.

This paper focuses on the research of NS-DBD plasma actuator on the control of increasing lift and reducing drag of two-section airfoil. The researches of NS-DBD plasma actuator on the control of flow separation of airfoil have been carried out extensively [29,30], but the research on multi-section airfoil is few. The control of flow separation, lift improvement, and drag reduction for multi-section airfoil is of great significance and value in practical engineering applications, especially in the takeoff and landing stages of aircraft.

In this paper, NS-DBD plasma actuators are arranged near the gap between the main wing and the flap, and the influence on the aerodynamic performance of the flap lift device is analysed by adjusting the discharge parameters of the actuator. This method has the advantages of simplicity, energy savings, and small size, and it is applicable to the case in which the space for mounting the actuator around the flap is relatively limited. To some extent, it can replace the traditional multi-element flap lift device, which has a complicated mechanism structure and additional weight. It can be referred to as a plasma flap.

## 2. Research Model and Grid Partition

The NASA (national aeronautics and space administration) airfoil GA(W)-1 and its 29% flap, which are the widely used classic high lift multi-element airfoil, are selected as the numerical simulation study object. The airfoil is characterized by large thickness (the maximum thickness reaches 17% of the chord length), blunt leading edge, and trailing edge stall. In the meantime, the airfoil has a completely turbulent boundary layer, which can provide a larger lift coefficient without flow separation, and the

shape of the flap gap has been optimized to better avoid flow separation. The outline of the airfoil GA(W)-1 and its flap are shown in Figure 1.

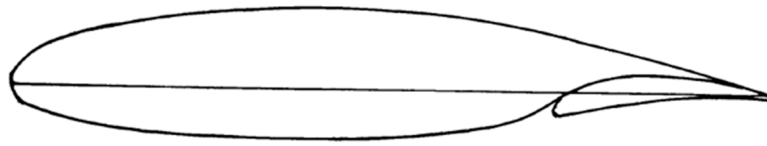


**Figure 1.** The airfoil GA(W)-1 and its 29% flap.

The chord length of the wing is 0.3 m, the chord length of the fowler flap is 29% of the total chord length, i.e., 0.087 m, and the chord length of the main wing except the flap is 0.288 m. The far-field inlet flow velocity is selected as 10 m/s, the Reynolds number is  $0.19 \times 10^6$ , and the boundary thickness of the first layer is calculated as  $1 \times 10^{-5}$  when  $Y^+$  is taken as 1. In this paper, a  $10^\circ$  flap deflection angle is selected as the research object, its parameters are defined by the orthogonal method, and the gap height is 0.075 m. Pointwise is used for grid partition, and after verifying the convergence of the grid, it is determined that the final amount of the grid is approximately 120,000. The grid structure is shown in Figure 2.

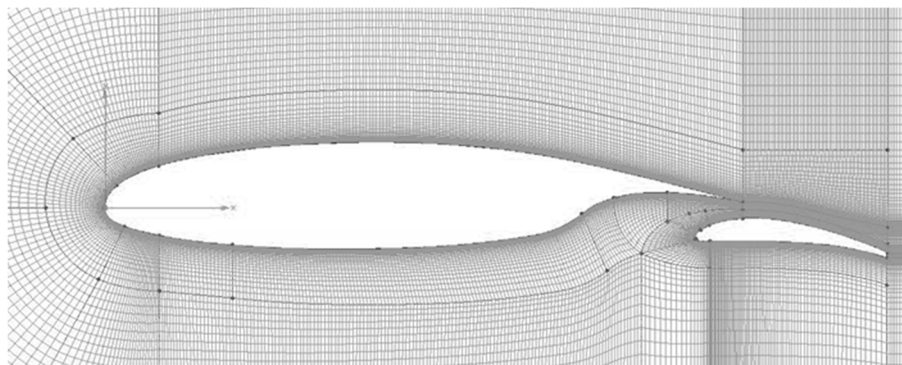


**Figure 2.** Mesh of the airfoil with a flap angle of  $10^\circ$ .

The density-based solver, SIMPLE algorithm, and second-order upwind format in Fluent are used for numerical calculation, and the standard  $k-\epsilon$  second-order model is used for the turbulence model. The Reynolds Averaged Navier–Stokes (RANS) model is used in this simulation.

This study needs to calculate the unsteady simulation of 25 pulse periods, and it is a high Reynolds number problem, the workload of calculation and simulation is very huge. The final overall effect of NS-DBD on the airfoil is focus, and the specific impact and instability of NS-DBD convection field are not concerned, so Large eddy simulation (LES) and direct numerical simulation (DNS) methods are not very suitable, although they can more accurately simulate the flow field changes at every moment, but the overall effect and time equalization effect of LES, DNS, and RANS are equivalent. Therefore, the RANS model can not only save resources and time, but also get ideal overall results. In addition, the RANS model has been widely accepted in the existing unsteady NS-DBD numerical simulation research. Kiyoshi et al. [31] in order to obtain detailed flow field changes and get the goal consistent with the engineering test results in the numerical study of shock/boundary layer separation controlled by NS-DBD, the method of RANS and LES was combined. LES is used to solve the generation and evolution of vortices, then momentum is transferred to the boundary layer, and RANS is used to calculate the rest of the region. The final results are in good agreement with the experimental values, and RANS can get the phenomena in the engineering experiments, including reflux, flow field change, and other issues. The detailed transient change of separation bubble depends on the LES model. The RANS model cannot get all the unsteady contents of the flow field, but this

does not hinder its advantages in simulating large-scale problems and the rationality consistent with the engineering experimental results. Similarly, Abdollahzadeh et al. [32] used RANS model to study the influence of DBD on ACHEON nozzle model by numerical simulation. Finally, the effect of DBD on flow separation and vectoring nozzle is consistent with the three-dimensional experimental results. Therefore, it is reasonable to use RANS model to carry out the unsteady simulation in engineering application research.

### 3. Discharge Position and Parameter Setting of the Plasma Actuator

In this paper, the plasma actuators are placed at three different positions near the flap, and the effect on the aerodynamic performance of the high lift device is analysed by adjusting the parameters of the actuators. The three discharge positions are: (1) The upper surface of the main wing near the trailing edge (abbreviated as the upper surface); (2) the upper surface of the main wing close to the trailing edge (abbreviated as the upper trailing edge); and (3) the lower surface of the main wing close to the trailing edge (abbreviated as the lower trailing edge). The specific locations are shown in Figure 3.

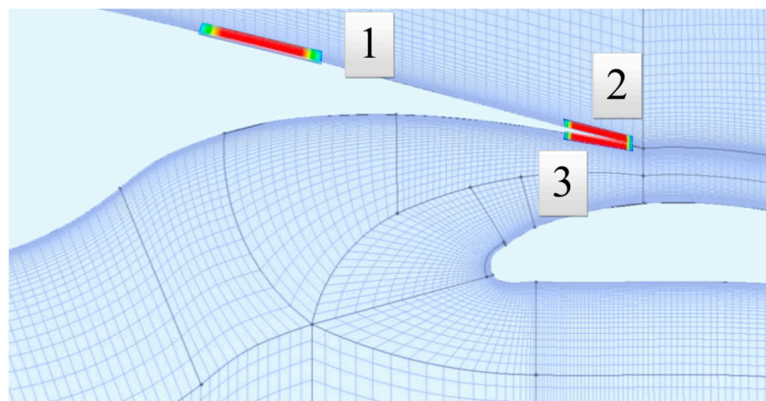


**Figure 3.** Discharge positions of DBD (dielectric barrier discharge) plasma actuators.

The numerical simulation for the plasma actuator based on the UDF programme approximates the pulse generated by the nanosecond discharge to the square wave signal, and the process of DBD discharge is simulated by adding a joule heat source in the discharge position. The influence of different parameters on the aerodynamic performance of the high lift device can be studied by changing the discharge frequency, pulse width, and number of heat sources in UDF. The value of joule heat applied to each grid cell requires a change of the heating file, which is read separately in the programme. In this paper, the three parameters of discharge frequency, pulse width, and energy density are selected to study the different effects of the NS-DBD plasma actuator applied to the flow control in the flap.

Since the dominant effect of the NS-DBD actuator is known to be the thermal effect (namely, Joule heating) [17,19,28], in the numerical simulation the effect of the discharge of the NS-DBD actuator is represented as instantaneous gas heating [33]. In this paper, the NS-DBD numerical simulation is based on phenomenological theory. During the NS-DBD discharge process, due to the short discharge time (on the order of ns), the body-force effect on the flow field is ignorable when compared to bulk-heating-induced effect. As a result, Joule heat is added as a source term to the energy equation by writing a UDF in Fluent. The two-dimensional unsteady, compressible Reynolds Average Navier–Stokes governing equations are as follows:

$$\frac{\partial \rho}{\partial t} + \nabla \cdot (\rho \mathbf{u}) = 0 \quad (1)$$

$$\frac{\partial (\rho \mathbf{u})}{\partial t} + \nabla \cdot (\rho \mathbf{u} \mathbf{u} + p \mathbf{I} - \boldsymbol{\tau}) = \mathbf{F} \quad (2)$$

$$\frac{\partial (\rho C_p T)}{\partial t} + \nabla \cdot (\rho \mathbf{u} C_p T - \nabla (k \nabla T)) = Q \quad (3)$$

where  $\boldsymbol{\tau} = \mu [\nabla \mathbf{u} + (\nabla \mathbf{u})^T - \frac{2}{3} (\nabla \cdot \mathbf{u}) \mathbf{I}]$ .

In the equations above,  $\rho$  is the density,  $p$  is the pressure,  $T$  is the temperature,  $C_p$  is the specific heat capacity at constant pressure,  $\mathbf{I}$ ,  $\mu$ , and  $k$  are the tensor unit, viscosity coefficient, and thermal conductivity, respectively.  $Q$  is the power density produced by the plasma discharge process. Body force  $\mathbf{F}$  is set to 0 due to its little effect on the flow field. The flow field is set as the ideal gas. The standard  $k$ - $\epsilon$  model is adopted in all simulations.

The intensity of the source representing the discharge of the NS-DBD actuator ( $Q$ ) is based on the result from the work by Ni [33] regarding a 15 kV voltage pulse, so the value of discharge voltage is 15 kV. The governing equation is solved with the density-based solver of the ANSYS 17.1 (FLUENT 17.1) software. The gas is assumed to be a perfect gas, and the coefficient of viscosity is calculated according to Sutherland's law.

## 4. Simulation Results and Analysis

### 4.1. Comparisons of Discharge Frequency

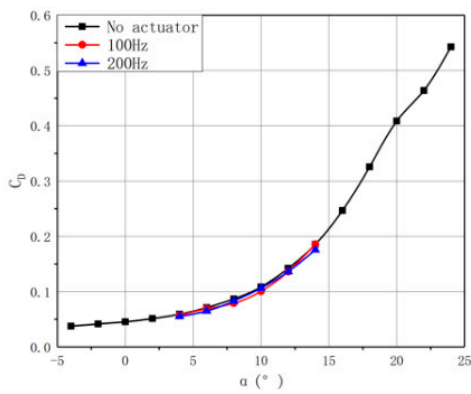
First, the effect of discharge frequency on the flap lift device is analysed, and two discharge frequencies, 100 and 200 Hz, are selected. The effects of different discharge frequencies at three different discharge positions (the upper surface, upper trailing edge, and lower trailing edge) under the 10° flap deflection angle are studied in this section. Other parameters, such as pulse width (50 ms) and discharge energy density ( $10^{13}$  W/m<sup>2</sup>), remain unchanged. Since the pulse action process is similar when only the discharge frequency is changed, in the comparative analysis of the flow field structure, only the vorticity distributions of the flow field after the first, 5th, 10th, and 20th pulse, which have more obvious distinctions, are selected.

#### 4.1.1. Comparison Results of the Aerodynamic Forces and Moments

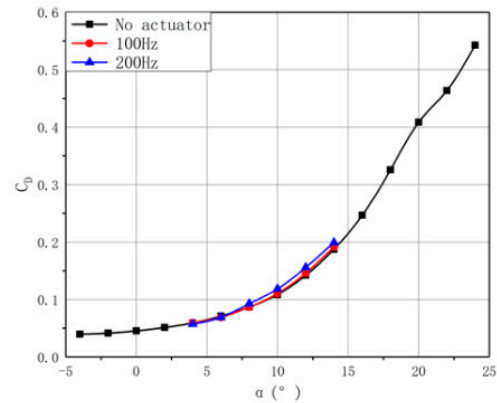
##### (1) Drag Coefficient

The control effects of the three selected discharge positions are not obviously different in the drag coefficient. Compared with the specific decrease value and the drag curve trend, it can be found that the lower trailing edge position has a better drag reduction effect, but increasing the discharge frequency will weaken the drag reduction effect, especially when the flow field has been obviously separated but not completely stalled at 8 and 10° angles of attack, and the reduction of drag generated by a 200 Hz discharge frequency is significantly lower than that generated by 100 Hz. The upper trailing edge discharge position leads to the increase of drag, the increase in frequency will strengthen this adverse effect, which makes the drag obviously greater than that without the discharge, and it is more likely for this trend to form in the case of large area of the separation flow. For the upper surface discharge position, the change of discharge frequency has no obvious influence on the drag coefficient, as shown in Figure 4.

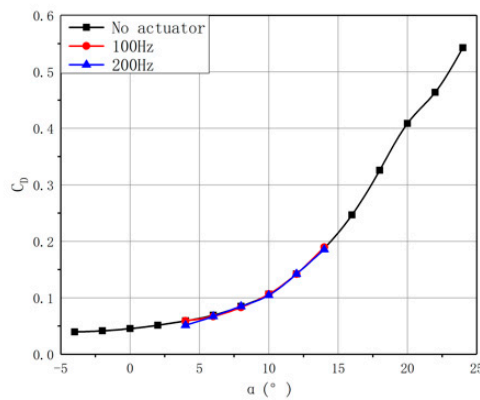
It can be inferred that the increase of discharge frequency improves the incentive efficiency to some extent, that is, the flow field under high-frequency excitation can be stabilized in a shorter period of time. However, there is no obvious advantage in the reduction of airfoil drag.



(a) Lower trailing edge discharge.



(b) Upper trailing edge discharge.



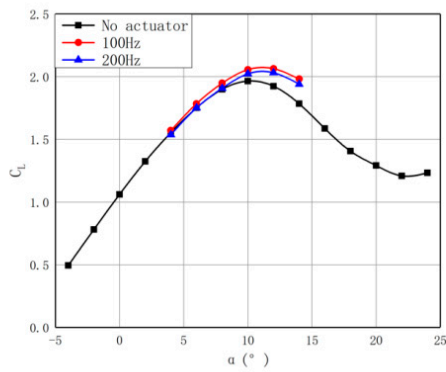
(c) Upper surface discharge.

Figure 4. The drag coefficient curve at different discharge frequencies.

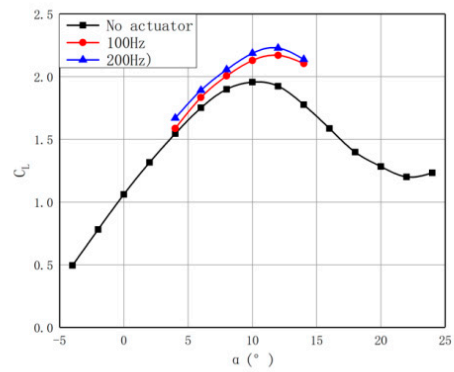
(2) Lift Coefficient

In terms of lift coefficient, the effect of the 200 Hz discharge frequency is different from that of 100 Hz at different positions: Weakening at the lower trailing edge, strengthening at the upper trailing edge, and no obvious effect at the upper surface. For the lower trailing edge discharge, when the frequency increases, the lift coefficient does not increase, and instead is actually slightly weakened, and the increment rate decreases with different degrees in the full range of angle of attack. For the upper trailing edge discharge, the increase in frequency can significantly increase the lift increment. For example, when the flow field at a 12° angle of attack has been separated, the lift increment can be increased from 12.85% to 15.8%. For the upper surface discharge, there is no obvious difference at the two discharge frequencies, as shown in Figure 5.

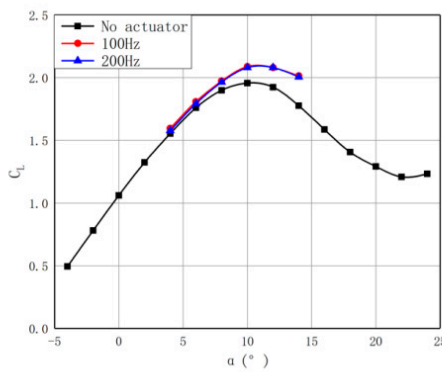
It can be inferred that, for the lower trailing edge discharge with a relatively limited effect of flow field range, increasing the frequency will not increase the lift, and even the effect of the flow field will decrease because the pulses pass through the gap (between the main wing and flap) too quickly. For the upper trailing discharge with large effect range and higher lift increment, the increase in frequency can strengthen this trend, which can result in quicker vortex shedding of the upper surface of the flap and more efficient effect of the pulse wave.



(a) Lower trailing edge discharge.



(b) Upper trailing edge discharge.

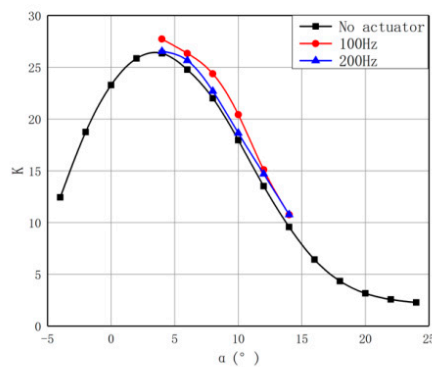


(c) Upper surface discharge.

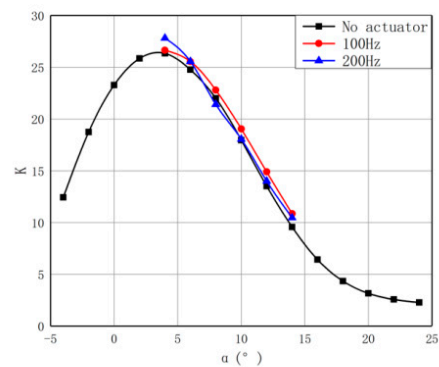
Figure 5. The lift coefficient curve at different discharge frequencies.

### (3) Lift-Drag Ratio

The three different discharge positions all show a law that the lift-drag ratio decreases as the discharge frequency increases, as shown in Figure 6. At the upper trailing edge position, there is little contribution to the lift-drag ratio near an 8° angle of attack at a 200 Hz discharge frequency.

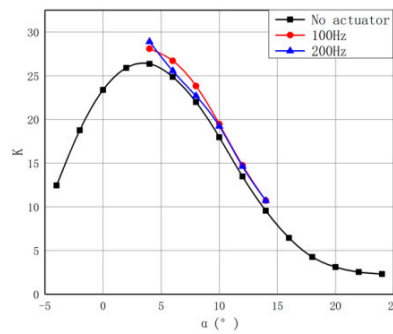


(a) Lower trailing edge discharge.



(b) Upper trailing edge discharge.

Figure 6. Cont.



(c) Upper surface discharge.

Figure 6. The lift-drag ratio curve at different discharge frequencies.

#### 4.1.2. Comparative Analysis of the Flow Field Structure

##### (1) Lower Trailing Edge Actuation

Figure 7 shows the influence of the intensity of the plasma aerodynamic actuation with the change of discharge frequency at the lower trailing edge from the perspective of vorticity. The size of the shedding vortex is smaller, and the diffusion speed is slower at a 200 Hz frequency. Observing the vorticity distribution after the first pulse, it can be seen that the shedding vortex caused by the 100 Hz discharge frequency has slipped to the middle part of the separation area on the upper surface of the flap, while the vortex generated by the 200 Hz discharge frequency has just started to touch the area of large vorticity. As seen from the vorticity distribution after the 5th, 10th, and 20th pulses, the vortices generated by the high-frequency discharge are more likely to accumulate on the upper surface of the flap, and the shedding speed is less than the low frequency (100 Hz), which causes the vortices generated by each pulse excitation to fail to separate from each other, forming a large vorticity area that has a larger area. Therefore, the integration and reattachment effect of the flow in the separation zone is not as good as that of the 100 Hz discharge frequency, which is also reflected in the aerodynamic force.

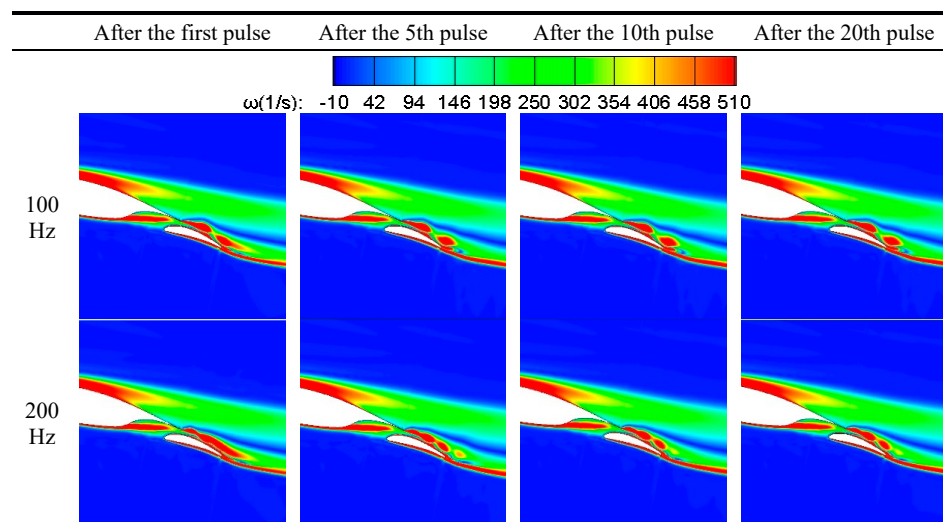
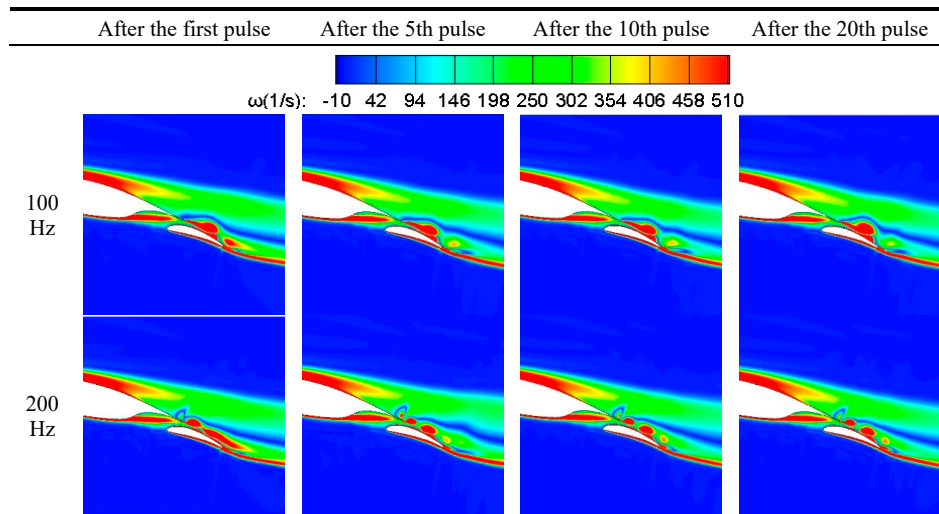


Figure 7. The vorticity distribution after the first, 5th, 10th, and 20th pulses, stimulated by the different discharge frequencies at the lower trailing edge position.

##### (2) Upper Trailing Edge Actuation

Figure 8 shows that the shedding vortex generated by the high frequency discharge at the upper trailing edge is different from that at the lower trailing edge. Although the vortices are also small in

size, they slide alone and independently from the upper surface of the flap instead of joining together. Compared with the 100 Hz pulse excitation, the 200 Hz discharge frequency has better control ability of the separation flow on the upper surface of the flap: The shedding vortex is small in size and close to the wing surface, while the size of the vortex caused by the 100 Hz discharge frequency is too large to be closely attached to the upper surface of the flap, and it is easier for it to cause a flow with a large vortex on the surface in the propagation process. Thus, the increase of the frequency has a positive effect on the pulse excitation. In addition, the velocity distribution shows that the final separation region is smaller when the frequency increases.



**Figure 8.** The vorticity distribution after the first, 5th, 10th, and 20th pulses, stimulated by the different discharge frequencies at the upper trailing edge position.

### (3) Upper Surface Actuation

The vorticity distribution caused by the upper surface pulse actuator when the discharge frequency changes is shown in Figure 9. The discharge at 200 Hz can cause more frequent vortex shedding. However, because the position of the pulse actuator has little influence on the flow area on the upper surface of the flap, the actual effect is not much different, even if there is a slight disturbance reflected in the vorticity distribution.

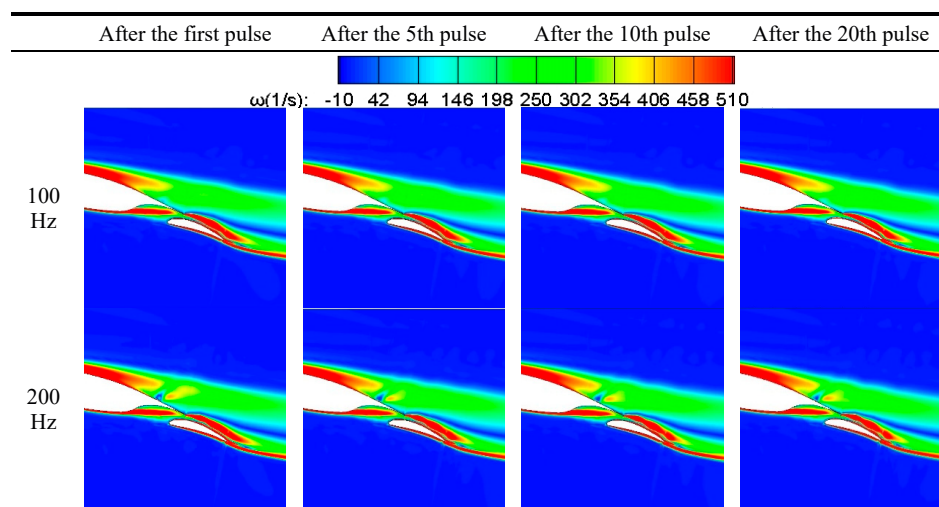


**Figure 9.** The vorticity distribution after the first, 5th, 10th, and 20th pulses, stimulated by the different discharge frequencies at the upper surface position.

In addition, the influence of the discharge frequency on the effect of the pulse actuator is also verified under the condition of the 20° flap deflection, and the results show a similar law to that of the 10° flap deflection.

#### 4.2. Comparisons of Discharge Pulse Width

Pulse width is the maximum duration of a single-nanosecond pulse during discharge. When the frequency is determined, and the period  $T$  of a single pulse is certain, a different pulse width  $W$  corresponds to a different duty cycle  $P$ , as shown in Formula (4).

$$W = T \times P \quad (4)$$

In this part, the actuator at the lower trailing edge is selected as the research object. Under the condition that the inlet wind speed is 10 m/s, the flap deflection angle is 10°, the discharge frequency is 100 Hz, and the discharge energy density is  $10^{13}$  W/m<sup>2</sup>, four discharge pulse widths are selected, that is, 50, 100, 200, and 500 ns.

##### 4.2.1. Comparison Results of Aerodynamic Forces and Moments

The plasma actuator at the trailing edge position has a weak influence on the drag coefficient. As shown in Figure 10, the influences of several different discharge pulse widths on the drag coefficient are compared. On the whole, in all conditions, the plasma actuators have a certain drag reduction effect, but all of them are weak. Among them, the discharge with the 100 ns pulse width has the maximum drag reduction when the angles of attack are 4 and 6° without large-scale flow separation. When the pulse width is 200 ns, there is the most obvious drag reduction effect at 8 and 10° angles of attack where flow separation has taken place, which is up to 15.49%.

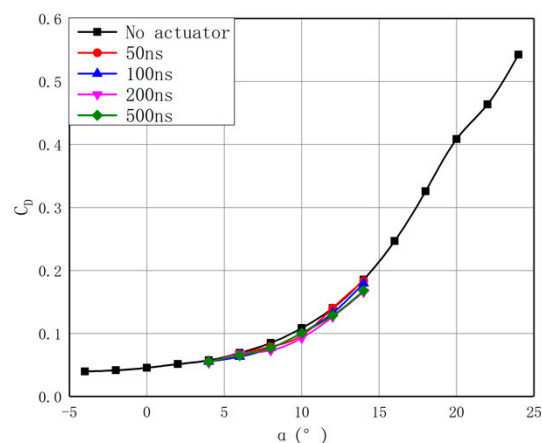


**Figure 10.** Drag coefficient curve of variable pulse width.

The effects of plasma actuators with different pulse widths on the lift coefficient are shown in Figure 11. The flow field under the plasma excitation has the effect of moving the stall point backward and has a certain effect of lift increase. The maximum lift coefficient occurs under the 50 ns pulse width discharge (up to 10.89% at a 14° angle of attack). From the curve trend, the 500 and 50 ns discharges have similar effects to delay stall, but the effects of the 100 and 200 ns discharges are more obvious. The 100 ns discharge significantly delays the maximum lift coefficient point from 10 to 12°, and the effect of lift increase is close to that of the 50 ns discharge (10.91% increase at a 14° angle of attack). The lift coefficient of the airfoil under the 200 ns discharge does not decrease rapidly when the angle of attack reaches 14°, indicating that the stall delay effect is obvious.

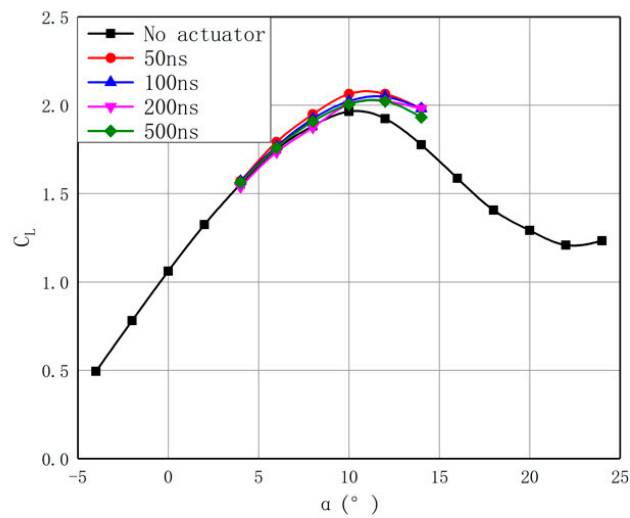


Figure 11. Lift coefficient curve of variable pulse width.

The effects of plasma actuators with different pulse widths on the lift-drag ratio are shown in Figure 12. Under the attack angles of 4 and 6° without flow separation, the 100 ns discharge has the best increase of the lift-drag ratio, up to 10.75%. When the flow field has separated at 8 to 14° angles of attack, the 200 ns discharge has the best increase of lift-drag, up to 21.55%.

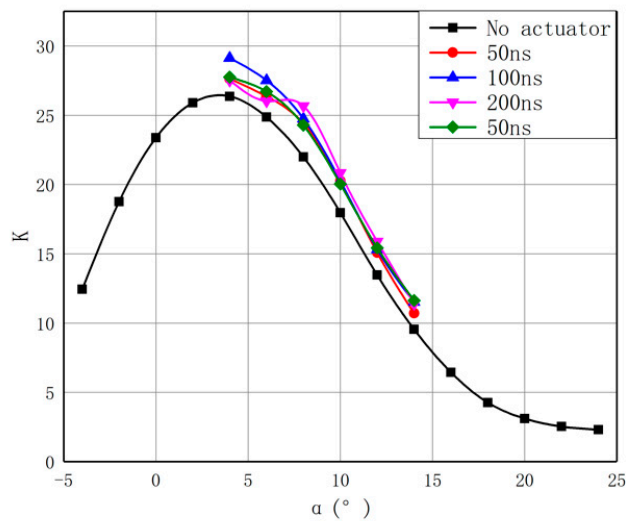


Figure 12. Lift-drag ratio coefficient curve of variable pulse width.

In conclusion, the pulse actuator working at 50 ns pulse width has a better effect on lift, but the 100 and 200 ns pulse widths have better comprehensive control ability.

#### 4.2.2. Comparative Analysis of the Flow Field Structure

Similarly, the flow field structure with a 12° angle of attack is selected. Four different moments of a single pulse are taken to analyse the effect differences at different moments. From the velocity distribution diagram (Figure 13), when the pulse width increases, the actual discharge time in a period increases, and the disturbance in the flow field also lasts longer, which will produce more obvious pulse waves. When the plasma actuator is applied to the lower surface of the main wing close to the trailing edge, the disturbance generated by the discharge will first interfere with the flow in the gap between the main wing and flap and then propagate forward and backward at the same time after

acting on the upper surface of the flap. The backward disturbance can effectively accelerate the flow on the upper surface of the flap, while the forward disturbance is contrary to the original flow direction, which does not help to reduce the drag. When the pulse width is small (50 and 200 ns), the forward pulse is quickly consumed, and the backward pulse reduces the low-speed zone on the upper surface of the flap and the trailing edge. When the pulse width is large (500 ns), the effect of discharge on the separated area is slightly better than that under the condition of small pulse width. However, when part of the energy flows to the upper and lower surface of the main wing, an arc-shaped wave with a large velocity gradient will be generated and advance to the leading-edge point, which is unfavourable. The pulse width of 200 ns obviously accelerates and integrates the separation flow in the low-speed zone, and it is not sufficiently strong to interfere the airflow above and below the main wing; therefore, the front and rear flow fields are well balanced, and relatively better the lift-drag ratio is obtained.

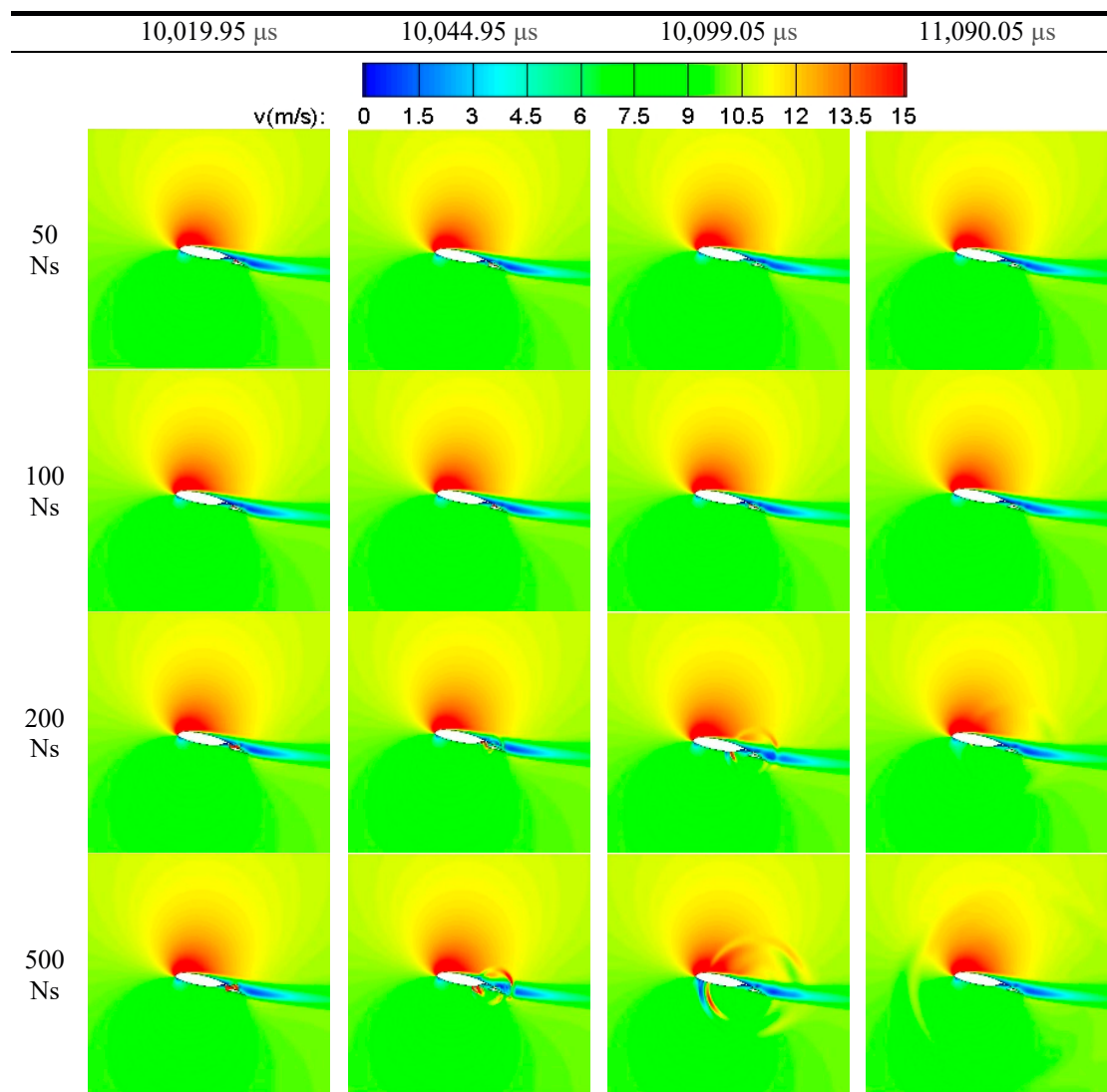


**Figure 13.** The velocity distribution under single pulse discharges with different pulse widths.

As seen from the vorticity distribution diagram (Figure 14), the increased pulse width can cause stronger vortex shedding and have a more obvious reduction effect on the large vorticity area on the upper surface of the flap. However, the upper and lower flow fields of the main wing are also more affected.

In terms of the vorticity of the concave zone in the lower gap of the main wing, the discharges with 50 and 100 ns pulse widths have appropriate perturbation effects on it, and in the process of the excitation spreading, the vorticity can be reduced obviously. The discharge with the 500 ns pulse width first completely breaks the vorticity here and then continues to spread forward, resulting in a strong vortex in the gap between the main wing and flap, which has an adverse effect on the flow.

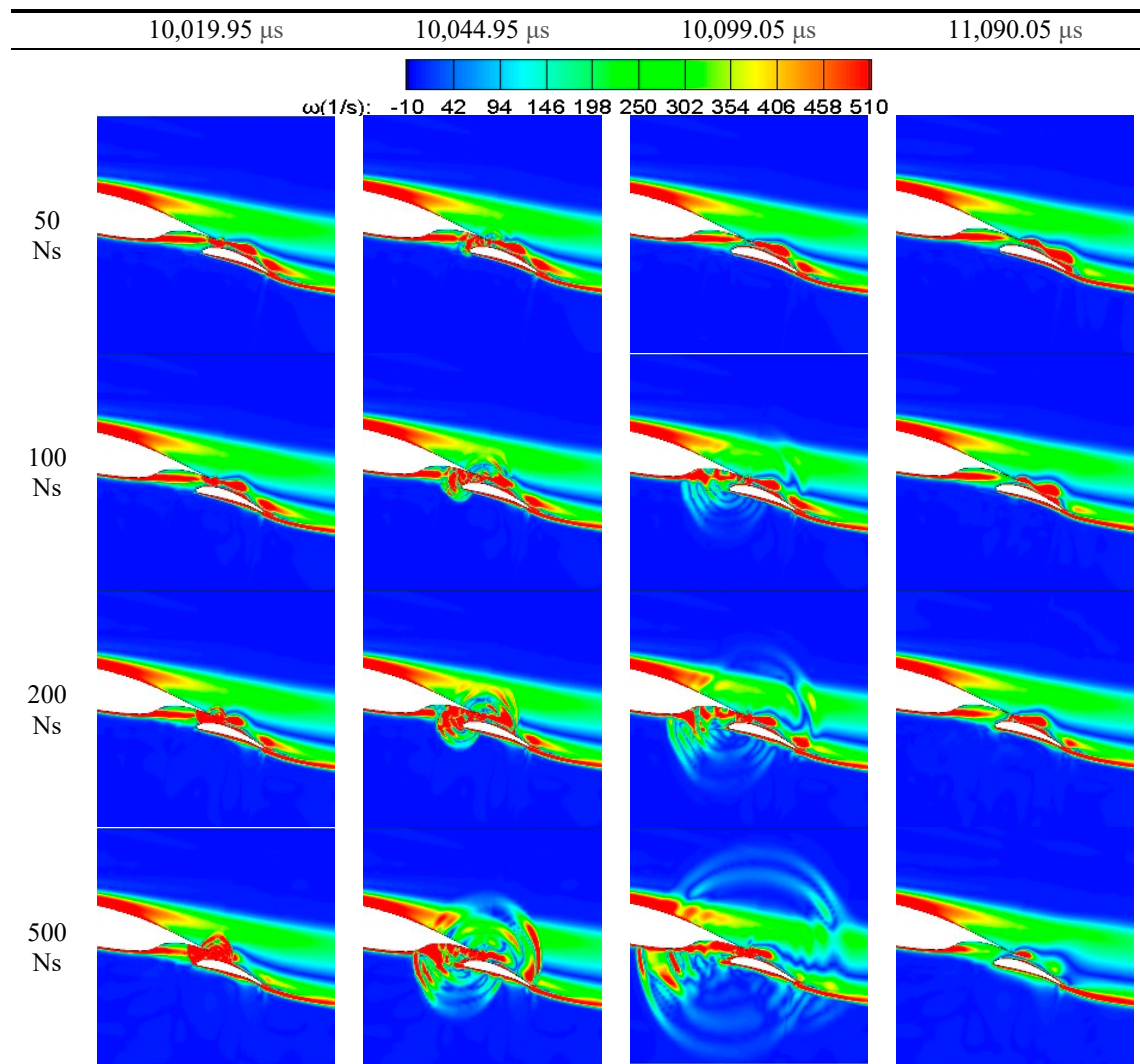


**Figure 14.** The vorticity distribution under single pulse discharges with different pulse widths.

From the pressure distribution diagram (Figure 15), the annular high-pressure area formed by the large pulse width discharge even has a multi-layer high-pressure area, and the duration is longer. Pressure fluctuations can also affect a wider range, extending to the upper and lower surfaces of the entire airfoil. When the pressure wave is about to dissipate, the disturbance effects of different pulse width discharges on the lower surface of the airfoil are similar. In the process of the propagation of the discharge pulses with 200 and 500 ns pulse widths, the high-pressure parts last too long, resulting in a very strong disturbance of the upper and lower flow field and have no obvious advantage in the pressure difference. It is not better than the small pulse width discharge in the increasement of lift.

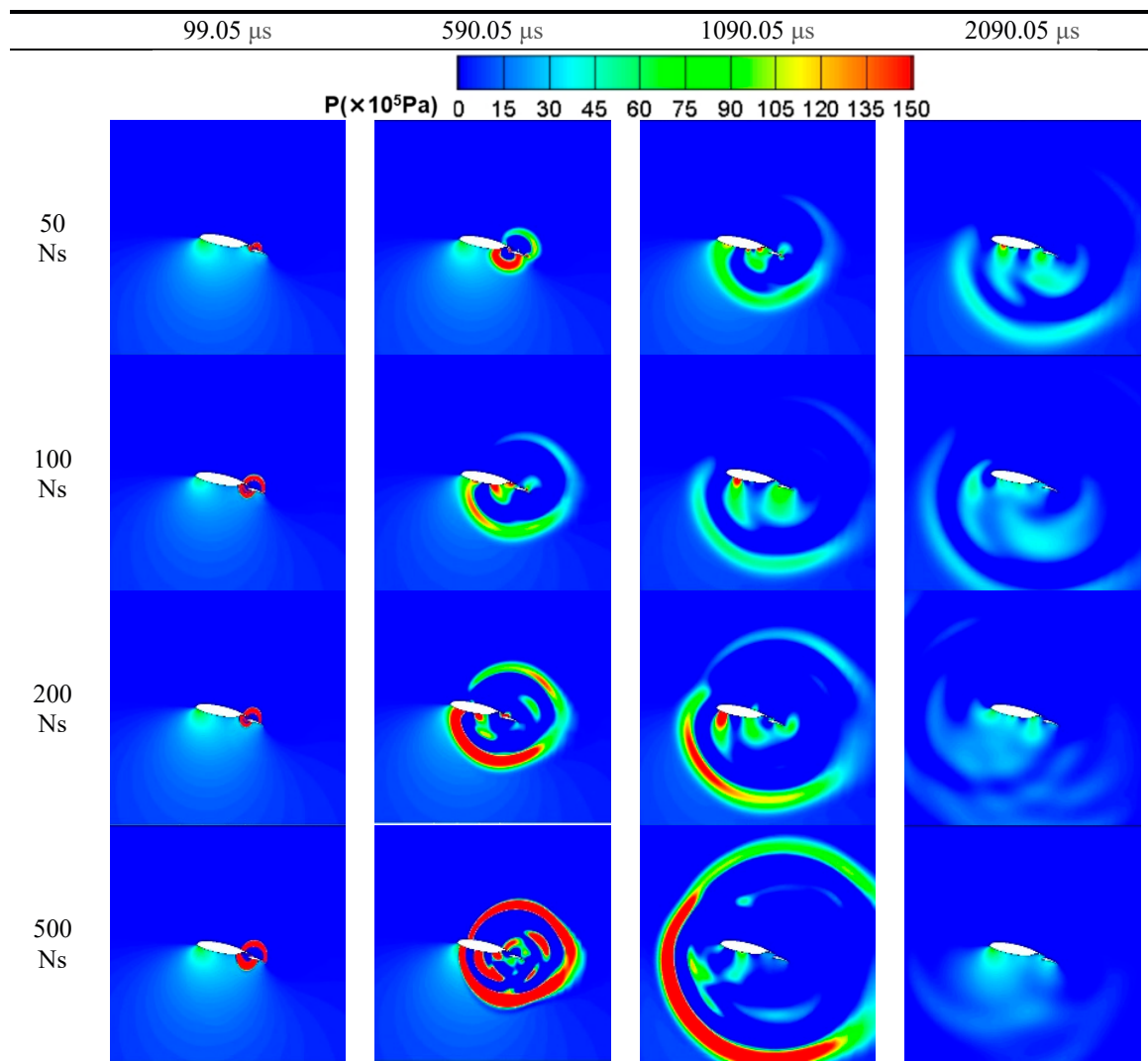


Figure 15. The pressure distribution under single pulse discharges with different pulse widths.

### 4.3. Discharge Energy

In practical application, there are many restrictions on the active flow control applied on the surface of the aircraft, and thus the discharge energy should not be too high and should be controlled within  $10^{14} \text{ W/m}^2$ . If the discharge energy exceeds the limit range, first it is easy to exceed the temperature limit in the numerical calculation and report error, and second, it is easy to cause the DBD electrode to break down and then burn out, and the existence of overly high temperature points is also not allowed in practical application.

In this part, the actuator at the lower trailing edge is also selected as the research object. When the inlet wind speed is 10 m/s, the flap deflection angle is  $10^\circ$ , the discharge frequency is 100 Hz, the pulse width is 50 ns, a discharge energy density of  $10^{13} \text{ W/m}^2$  is adopted, and an attempt is made to increase the energy to  $10^{14} \text{ W/m}^2$  to observe whether the plasma actuator performs better in higher energy density under the condition of no breakdown.

#### 4.3.1. Comparison Results of Aerodynamic Forces and Moments

Figure 16 shows that the change of discharge energy has no significant influence on the drag reduction caused by the plasma actuator; the drag coefficient curves have the same trend. According to the specific data, enhancing the discharge energy under the angles of attack of  $4^\circ$  and  $6^\circ$  without flow

separation can reduce the drag more effectively to a certain extent. After large area separation of the airflow, this effect is correspondingly weakened. On the whole, the drag reduction of  $10^{14} \text{ W/m}^2$  is slightly larger than that of  $10^{13} \text{ W/m}^2$ .

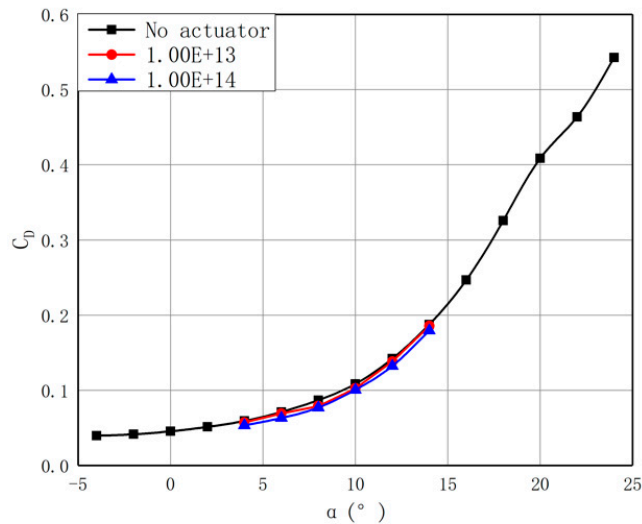


Figure 16. Drag coefficient curve of variable energy.

It can be seen from Figure 17 that the influence of energy increase on the lift coefficient is not optimistic. The two curves have the same trend, but the curve of the larger discharge energy always lies below the curve of the smaller discharge energy, which can show that the discharge energy increase does not enhance the lift of the airfoil.

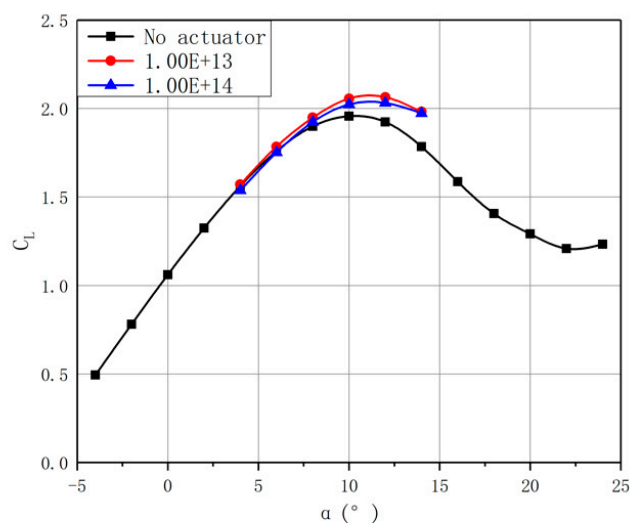


Figure 17. Lift coefficient curve of variable energy.

Figure 18 shows the different lift-drag ratios under different discharge energies. When the flow field is not separated, the lift-drag ratio can be increased from 6.04% to 10.75% by increasing the discharge energy. When a flow separation zone of large area occurs above the airfoil, this effect is weakened to some extent, and from the curve, they basically coincide with each other and have little difference in numerical value. Mainly because the discharge with  $10^{14} \text{ W/m}^2$  energy density has a better drag reduction effect, it has a slight advantage in the lift-drag ratio.

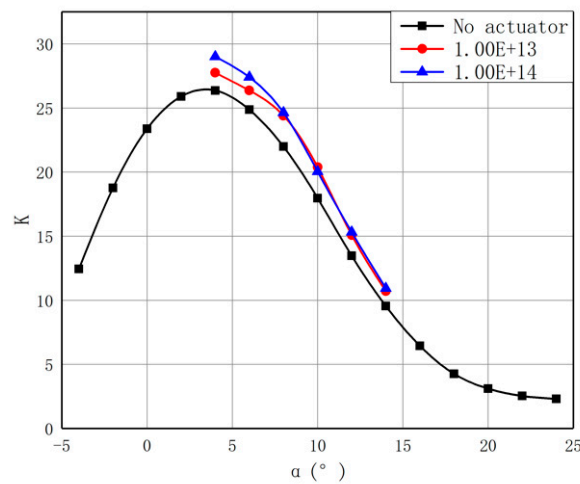


Figure 18. Lift-drag ratio curve of variable energy.

#### 4.3.2. Comparative Analysis of the Flow Field Structure

A single discharge pulse after the actuator is turned on is selected as a reference to illustrate the different effects of different discharge energies on the flow separation zone. Figure 19 shows the change in velocity distribution. When the discharge energy is improved by one order of magnitude, the pulse intensity increases significantly, and the disturbance velocity and vortex strength are obviously higher than those of the low discharge energy. The disturbance of the low-speed zone and vortex structure on the upper surface of the flap is also significantly stronger than that in the case of low discharge energy, which can integrate the separation zone faster to make the flow reattach, thus having a more obvious effect on drag reduction. From the change of vorticity distribution (Figure 20), with the increase of discharge energy, the vortex falls off and slides downstream faster, and the destruction to the vortex structure near the actuator is stronger. Although it is better in enhancing and accelerating the separated flow and vortex shedding, it has some adverse effects on some unrelated vortex structures. From the pressure distribution in Figure 21, it is also obvious that there is a huge difference in different discharge energies. The higher energy pulse propagates faster, covers a larger range, and has a greater impact on the pressure distribution. However, overly strong energy can easily cause the actuator to breakdown and lose efficacy.

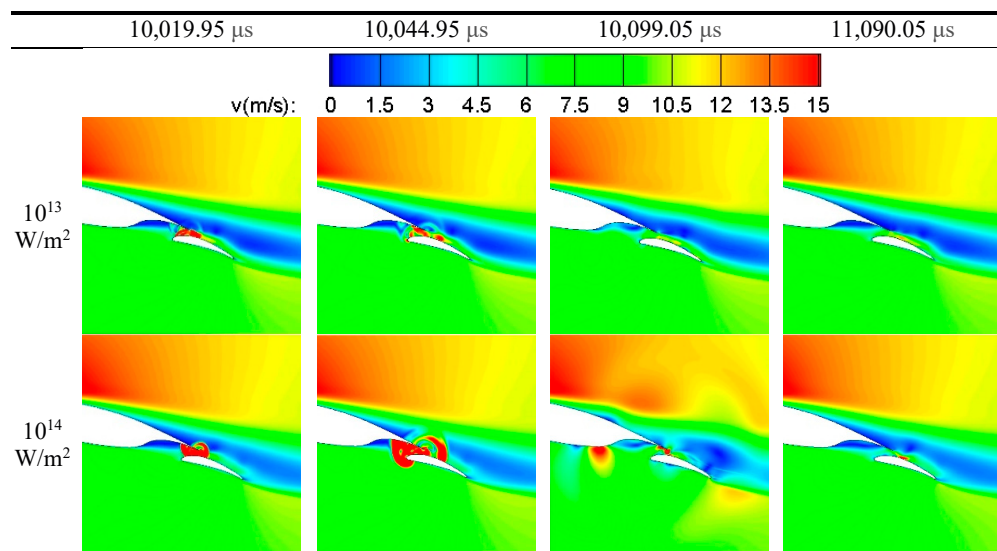


Figure 19. The velocity distribution under single pulse discharges with different energy densities.

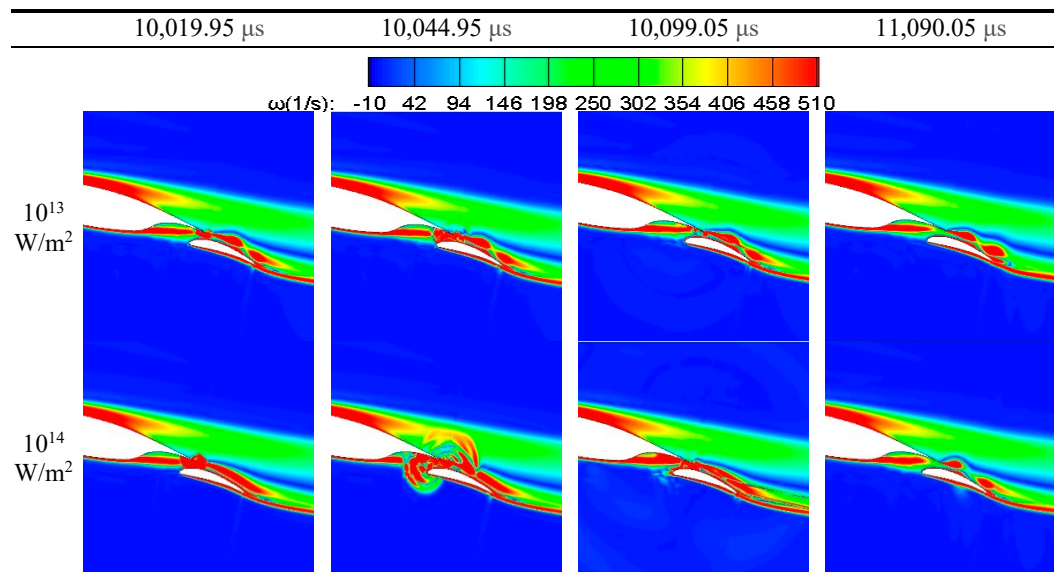


Figure 20. The vorticity distribution under single pulse discharges with different energy densities.

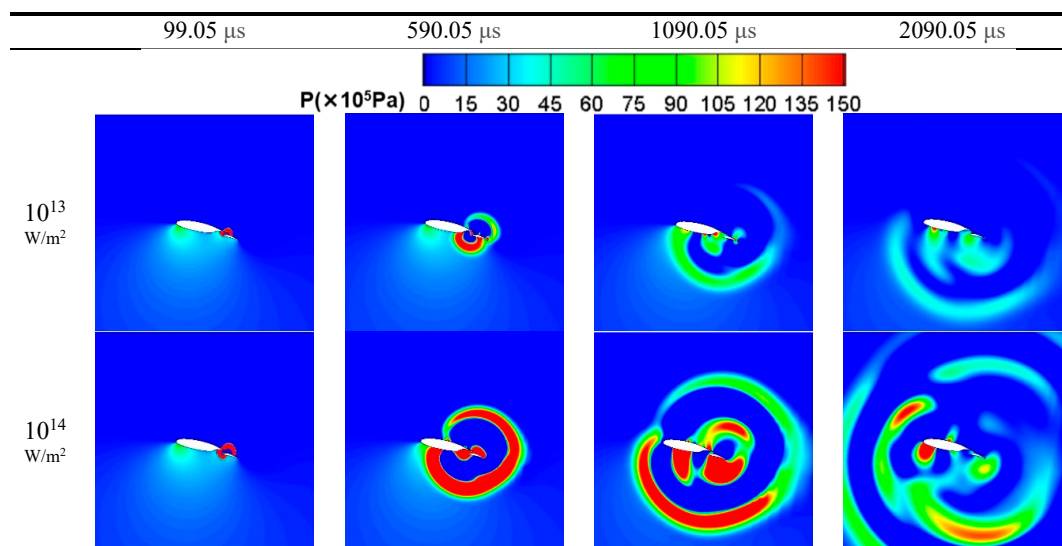


Figure 21. The pressure distribution under single pulse discharges with different energy densities.

### 5. Conclusions

In this paper, the effects of three discharge parameters of the NS-DBD plasma actuator, i.e., the frequency, pulse width, and energy, on the flow field control of the flap lift device are studied and discussed. From the comparison and analysis of the aerodynamic change and flow field structure, the results show the following:

(1) Comparisons of different discharge frequencies at three discharge positions. The increase of frequency has a position effect on the drag reduction at different positions, but the effect on the lift coefficient is different: The lift increment decreases at the lower trailing edge, the lift increment increases at the upper trailing edge, and the lift coefficient changes little at the upper surface. Therefore, the lift-drag ratio decreases when the frequency increases. It can be inferred that the increase of frequency cannot improve the excitation effect at the position where the original excitation effect is general, while it can enhance the original control effect at the position with obvious control effect. On the whole, the discharge frequency of 200 Hz is not better than 100 Hz, and the optimal discharge frequency needs to be further studied and analysed.

(2) The increase of discharge pulse width has a more significant effect on the flow field. A proper increase of pulse width can yield a better drag reduction effect and lift increase effect after stall, but when the pulse width is too large (500 ns), the control effect will be worse. After our comparison, it is found that the comprehensive excitation effect is better when the discharge pulse width is 100 and 200 ns, which are reference values for subsequent research.

(3) While the increase of discharge energy enhances the perturbation of the pulse, it also contributes to some adverse effects. It does not optimize the control efficiency of lift increase and drag reduction. When the discharge energy is too small, it is difficult to achieve the control effect because the disturbance decays too quickly. In addition, the increase of discharge energy is likely to lead to the high temperature of the flow field and the breakdown of the actuator, so in regard to the discharge energy, it is not true that larger is better. Therefore, further analysis is needed based on specific cases.

**Author Contributions:** Conceptualization: C.K. and Z.-W.S., Methodology: C.-Y.W., Data Curation: C.-Y.W., Formal Analysis: K.C. and C.-Y.W., Writing—Original Draft Preparation: K.C. and C.-Y.W., Writing—Review & Editing: K.C. and Z.-W.S.

**Funding:** This work was supported by the National Defense Pre-Research Foundation of China (Grant No. KO21021), the Foundation of the National Key Laboratory of Transient Physics, and the Foundation of the Defense Technology Innovation Special Field.

**Acknowledgments:** We are very grateful to Geng Xi and Du Hai for their help in the research process and the financial support provided by the national defense pre-research foundation of China. Finally, I would like to thank the reviewers and editors for their suggestions and help in the process of revision.

**Conflicts of Interest:** The authors declare no conflict of interest.

## References

1. Salvador, I.I.; Minucci, M.A.; Toro, P.G.; Oliveira, A.C.; Channes, J.B., Jr.; Myrabo, L.N.; Nagamatsu, H.T. Experimental Analysis of Heat Flux to a Blunt Body in Hypersonic Flow with Upstream Laser Energy Deposition—Preliminary Results. *AIP Conf. Proc.* **2006**, *830*, 163–171.
2. Takaki, R.; Liou, M.S. Parametric Study of Heat Release Preceding a Blunt Body in Hypersonic Flow. *AIAA J.* **2002**, *40*, 501–509. [[CrossRef](#)]
3. Falempin, F.; Firsov, A.A.; Yarantsev, D.A.; Goldfeld, M.A.; Timofeev, K.; Leonov, S.B. Plasma Control of Shock Wave Configuration in Off-design Mode of  $M = 2$  inlet. *Exp. Fluids* **2015**, *56*, 54. [[CrossRef](#)]
4. Boesch, G.; Vo, H.D.; Savard, B.; Wanko-Tchatchouang, C.; Mureithi, N.W. Flight Control Using Wing-Tip Plasma Actuation. *J. Aircr.* **2010**, *47*, 1836–1846. [[CrossRef](#)]
5. Seraudie, A.; Vermeersch, O.; Arnal, D. DBD Plasma Actuator Effect on a 2D Model Laminar Boundary Layer. In Proceedings of the Transition Delay under Ionic Wind Effect: 29th AIAA Applied Aerodynamics Conference, Honolulu, HI, USA, 27–30 June 2011.
6. Takahashi, H.; Liu, F.; Palavicini, M.; Oyarzun, M.; Griffin, J.; Ukeiley, L.; Cattafesta, L. Progress on Active Control of Open Cavities. In Proceedings of the 49th AIAA Aerospace Sciences Meeting Including the New Horizons Forum and Aerospace Exposition, Orlando, FL, USA, 4–7 January 2011.
7. Wang, J.; Li, H.; Meng, X.; Zhang, D.; Liu, F.; Luo, S. Nanosecond-SDBD Actuation Over a Conical Forebody at Wind Speed 72 m/s and Angle of Attack 45 Degree. In Proceedings of the 33rd AIAA Applied Aerodynamics Conference, Dallas, TX, USA, 22–26 June 2015.
8. Otsu, H.; Kamada, Y.; Yamagiwa, Y.; Ohno, T. Attitude Control of UAV Using DBD Plasma Actuator. In Proceedings of the 27th International Congress of the Aeronautical Sciences, Nice, France, 19–24 September 2010.
9. Kriegseis, J.; Oiler, B.M.; Grundmann, S.; Tropea, C. Light Emission, Discharge Capacitance and Thrust Production of DBD Plasma Actuators. In Proceedings of the 49th AIAA Aerospace Sciences Meeting including the New Horizons Forum and Aerospace Exposition, Orlando, FL, USA, 4–7 January 2011.
10. Zhao, X.; Li, Y.; Yue, T.; Wu, Y.; Zhu, T.; Luo, Z. Experimental Study of Plasma Aerodynamic Excitation for Suppressing Flow Separation in High-load Compressor Cascades. *High-Voltage Technol.* **2011**, *37*, 1521–1528.

11. Patel, M.P.; Sowle, Z.H.; Corke, T.C.; He, C. Autonomous Sensing and Control of Wing Stall Using a Smart Plasma Slat. *J. Aircr.* **2007**, *44*, 516–535. [[CrossRef](#)]
12. Dawson, R.; Little, J. Characterization of Nanosecond Pulse Driven Dielectric Barrier Discharge Plasma Actuators for Aerodynamic Flow Control. *J. Appl. Phys.* **2013**, *113*, 103302. [[CrossRef](#)]
13. Little, J.; Takashima, K.; Nishihara, M.; Adamovich, I.; Samimy, M. Separation Control with Nanosecond-Pulse-Driven Dielectric Barrier Discharge Plasma Actuators. *AIAA J.* **2012**, *50*, 350–365. [[CrossRef](#)]
14. Correale, G.; Popov, I.; Rakitin, A.; Starikovskii, A.; Hulshoff, S.; Veldhuis, L. Flow Separation Control on Airfoil With Pulsed Nanosecond Discharge Actuator. In Proceedings of the 49th AIAA Aerospace Sciences Meeting including the New Horizons Forum and Aerospace Exposition, Orlando, FL, USA, 4–7 January 2011.
15. Wu, Y. Nanosecond pulsed discharge plasma actuation: Characteristics and flow control performance. In Proceedings of the 45th AIAA Plasmadynamics and Lasers Conference, Atlanta, GA, USA, 16–20 June 2014.
16. Rethmel, C.; Little, J.; Takashima, K.; Sinha, A.; Adamovich, I.; Samimy, M. Flow Separation Control over an Airfoil with Nanosecond Pulse Driven DBD Plasma Actuators. In Proceedings of the 51st AIAA Aerospace Sciences Meeting including the New Horizons Forum and Aerospace Exposition, Grapevine, TX, USA, 7–10 January 2013.
17. Roupassov, D.V.; Nikipelov, A.A.; Nudnova, M.M.; Starikovskii, A.Y. Flow Separation Control by Plasma Actuator with Nanosecond Pulsed-Periodic Discharge. *AIAA J.* **2009**, *47*, 168–185. [[CrossRef](#)]
18. Popov, I.; Nikipelov, A.; Pancheshnyi, S.; Correale, G.; Hulshoff, S.; Veldhuis, L.; Zaidi, S.; Starikovskiy, A. Experimental Study and Numerical Simulation of Flow Separation Control with Pulsed Nanosecond Discharge Actuator. In Proceedings of the 51st AIAA Aerospace Sciences Meeting including the New Horizons Forum and Aerospace Exposition, Grapevine, TX, USA, 7–10 January 2013.
19. Little, J.; Nishihara, M.; Adamovich, I.; Samimy, M. Separation Control From the Flap of a High-lift Airfoil Using DBD Plasma Actuators. In Proceedings of the 47th AIAA Aerospace Sciences Meeting including The New Horizons Forum and Aerospace Exposition, Orlando, FL, USA, 5–8 January 2009; p. 145.
20. Little, J.; Nishihara, M.; Adamovich, I.; Samimy, M. High-lift Airfoil Trailing Edge Separation Control Using a Single Dielectric Barrier Discharge Plasma Actuator. *Exp. Fluids* **2010**, *48*, 521–537. [[CrossRef](#)]
21. Little, J.; Mo, S. High-lift Airfoil Separation with Dielectric Barrier Discharge Plasma Actuation. *AIAA J.* **2015**, *48*, 2884–2898. [[CrossRef](#)]
22. Wang, W.B.; Zhang, R.P.; Huang, Z.B.; Huang, Y.; Wang, X.N.; Shen, Z.H.; Zhang, X. Experimental Study of Plasma Excitation for Two-stage Airfoil Lift. *J. Aerodyn.* **2012**, *31*, 64–68.
23. Benard, N.; Zouzou, N.; Claverie, A.; Sotton, J.; Moreau, E. Optical Visualization and Electrical Characterization of Fast-rising Pulsed Dielectric Barrier Discharge for Airflow Control Applications. *J. Appl. Phys.* **2012**, *111*, 33303. [[CrossRef](#)]
24. Li, Y.; Zhao, X.H.; Li, Y.H.; Chen, F.; Song, H.M. Large-Volume Nanosecond Pulse Lasting Discharge. *IEEE Trans. Plasma Sci.* **2011**, *39*, 2598–2599. [[CrossRef](#)]
25. Zheng, J.G.; Zhao, Z.J.; Li, J.; Cui, Y.D.; Khoo, B.C. Numerical Simulation of Nanosecond Pulsed Dielectric Barrier Discharge Actuator in a Quiescent Flow. *Phys. Fluids* **2014**, *26*, 36102. [[CrossRef](#)]
26. Leonov, S.B.; Yarantsev, D. Near-Surface Electrical Discharge in Supersonic Airflow: Properties and Flow Control. *J. Propuls. Power* **2008**, *24*, 1168–1181. [[CrossRef](#)]
27. Sergey, B.; Leonov, V.P. Dynamics of Energy Coupling and Thermalization in Barrier Discharges over Dielectric and Weakly Conducting Surfaces on  $\mu$ s to ms Time Scales. *J. Phys. D Appl. Phys.* **2014**, *47*, 465201.
28. Unfer, T.; Boeuf, J.P. Modeling and Comparison of Sinusoidal and Nanosecond Pulsed Surface Dielectric Barrier Discharges for Flow Control. *Plasma Phys. Control. Fusion* **2010**, *52*, 124019. [[CrossRef](#)]
29. Feng, L.H.; Jukes, T.N.; Choi, K.S.; Wang, J.J. Flow Control Over a NACA 0012 Airfoil Using Dielectric-barrier-discharge Plasma Actuator with a Gurney Flap. *Exp. Fluids* **2012**, *52*, 1533–1546. [[CrossRef](#)]
30. Zhao, G.Y.; Li, Y.H.; Liang, H.; Han, M.H.; Hua, W.Z. Control of Vortex on a Non-slender Delta Wing by a Nanosecond Pulse Surface Dielectric Barrier Discharge. *Exp. Fluids* **2015**, *56*, 1864. [[CrossRef](#)]
31. Kinefuchi, K.; Starikovskiy, A.Y.; Miles, R.B. Numerical Investigation of Nanosecond Pulsed Plasma Actuators for Control of Shock-wave/Boundary-layer Separation. *Phys. Fluids* **2018**, *30*, 106105. [[CrossRef](#)]

32. Abdollahzadeh, M.; Rodrigues, F.; Pascoa, J.C.; Oliveira, P.J. Numerical Design and Analysis of a Multi-DBD Actuator Configuration for the Experimental Testing of ACHEON Nozzle Model. *Aerosp. Sci. Technol.* **2015**, *41*, 259–273. [[CrossRef](#)]
33. Ni, F.Y.; Shi, Z.W.; Du, H. Numerical Simulation of Nanosecond Pulse Plasma Actuator for High Speed Flow Control of Cylinder. *Acta Aeronaut. Sin.* **2014**, *35*, 657–665.



© 2019 by the authors. Licensee MDPI, Basel, Switzerland. This article is an open access article distributed under the terms and conditions of the Creative Commons Attribution (CC BY) license (<http://creativecommons.org/licenses/by/4.0/>).